British Journal of Medicine & Medical Research
4(14): 2661-2683, 2014

SCIENCEDOMAIN *international*
www.sciencedomain.org

A Novel High-strength GIC System Composed of Poly (Acrylic Acid) With Different Molecular Architectures

Dong Xie[1*], Jun Zhao[1], Yiming Weng[1] and Jun Sun[1]

[1]Department of Biomedical Engineering, Purdue School of Engineering and Technology Indiana University-Purdue University at Indianapolis, Indianapolis, IN 46202, USA.

Authors' contributions

This work was carried out in collaboration among all authors. Author DX designed the study, supervised the students and wrote the manuscript. Author JZ performed a majority of experiments including synthesis, characterization, mechanical testing and data analysis. Author YW performed material and graph preparation. JS performed the biocompatibility test. All authors read and approved the final manuscript.

Original Research Article

Received 28th December 2013
Accepted 5th February 2014
Published 24th February 2014

ABSTRACT

Aims: The objective of this study was to synthesize and characterize the poly (acrylic acid) or PAA with different molecular architectures, use these polymers to formulate the cements with glass fillers, and evaluate the mechanical strengths of the formed cements.
Materials and Methods: The novel poly (acrylic acid)s with different molecular architectures were synthesized via ATRP technique. The reaction kinetics was studied. The formed cements were evaluated using compression, diametral compression, and 3-point bending, fracture toughness, knoop hardness, and wear resistance tests. The experimental cement was also evaluated for its in vitro biocompatibility.
Results: The results showed that either hyperbranched or star-hyperbranched polymer synthesis proceeds more slowly at the early stage but accelerates more quickly at the later stage than the star-shaped polymer synthesis. The higher the arm number and initiator concentration, the faster the ATRP reaction. It was also found that the higher the arm number and branching that the polymer had, the lower the viscosity of the polymer aqueous solution and the lower the mechanical strengths of the formed cement exhibited. The mechanical strengths of all three experimental glass-ionomer cements were very

**Corresponding author: Email: dxie@iupui.edu;*

similar to each other but much higher than those of Fuji II LC. The aging study showed that all the experimental cements increased their CS continuously during 30 days, unlike Fuji II LC. This novel cement system was proven to be in vitro biocompatible because it showed no any noticeable cytotoxicity to human dental pulp cells and mouse 3T3 mouse fibroblasts.

Keywords: Poly (acrylic acid); light-cured glass-ionomer cement; molecular architecture; viscosity; mechanical strength.

1. INTRODUCTION

There are three major dental filling restoratives including dental amalgam, composite resins and glass-ionomer cements. Glass-ionomer cements (GICs) are one of the most promising restoratives in dentistry [1]. Since their invention, these cements have been successfully applied in dentistry for more than 35 years [1-4]. The success of these cements is attributed to their unique properties such as direct adhesion to tooth structure and base metals [5,6], anticariogenic properties due to release of fluoride [7], thermal compatibility with tooth enamel and dentin because of low coefficients of thermal expansion similar to that of tooth structure [8], minimized microleakage at the tooth-enamel interface due to low shrinkage [8], and low cytotoxicity [9,10].

An acid-base reaction between calcium and/or aluminum cations released from a reactive glass and carboxyl anions pendent on polyacid describes the setting and adhesion mechanism of GICs [2,11]. Despite numerous advantages, brittleness, low tensile and flexural strengths have limited the current GICs for use only at certain low stress-bearing sites such as Class III and Class V cavities [1,2]. Much effort has been made to improve the mechanical strengths of GICs [1,4,11] and the focus has been mainly on improvement of polymer backbone or matrix [1,4,11,12-18]. Briefly two main strategies have been applied. One is to incorporate hydrophobic pendent (meth) acrylate moieties onto the polyacid backbone to make it become light- or redox-initiated resin-modified GIC (RMGIC) [12-15,17] and the other is to directly increase molecular weight (MW) of the polyacid [16-18]. As a result, the former has shown significantly improved tensile and flexural strengths as well as handling properties [12-15,17]. The strategy of increasing MW of the polyacid by either introducing amino acid derivatives or N-vinylpyrrolid one has also shown enhanced mechanical strengths [16-18]; however, the working properties were somehow worsen because strong chain entanglements formed in these high MW linear polyacids resulted in an increased solution viscosity [16,18]. It is known that viscosity is inversely proportional to MW of a polymer and a polymer with high MW often show both high mechanical strengths and viscosity [2]. So far, all the polyacids used in commercial GIC formulations have been linear polymers and using high MW of these linear polyacids has been limited due to the viscosity issue.

Polymers with star, hyperbranched or dendritic shapes often demonstrate low solution or melt viscosity because these molecular structures behave similar to a solution of hard spheres and exhibit limited chain entanglements, which is beneficial to polymer processing [19,20]. Recently, we have developed a light-curable glass-ionomer system composed of the 4-arm star polymer [21]. The polymer was synthesized via an advanced polymerization technique - atom-transfer radical polymerization (ATRP). The formed GIC system has no monomer in it. Because of this unique nature, the system has demonstrated substantially

higher mechanical strengths as compared to Fuji II LC [21,22]. The main purpose of using star-shaped polymer was to improve the mechanical strengths of the current GICs by altering the molecular architecture of the polymer. The strategy has been found valid [21,22]. In this paper, we have described synthesis and evaluation of the polymers with different molecular architectures including star-shaped, hyperbranched and star-hyperbranched polymers and compared the mechanical properties of the formed cements.

The objective of this study was to synthesize and characterize the poly (acrylic acid) or PAA with different molecular architectures, use these polymers to formulate the cements with glass fillers, and evaluate the mechanical strengths of the formed cements.

2. MATERIALS AND METHODS

2.1 Materials

2-Hydroxyl ethyl acrylate (HEA), 2-bromoisobutyryl bromide (BIBB), pentaerythritol, 1,1,1-tris-(hydroxymethyl)-propane, dipentaerythritol, triethylamine (TEA), pyridine, CuBr, N,N,N',N'',N''-pentamethyldiethylenetriamine (PMDETA), dl-camphoroquinone (CQ), 2-(dimethylamino)ethyl methacrylate (DMAEMA), butylated hydroxytoluene (BHT), tert-butyl acrylate (t-BA), glycidyl methacrylate (GM), hydrochloric acid (37%), diethyl ether, dioxane, N, N-dimethylformamide (DMF) and tetrahydrofuran (THF) were used as received from VWR International Inc (Bristol, CT) without further purifications. Fuji II LC cement and Fuji II LC glass powders were used as received from GC America Inc (Alsip, IL).

2.2 Synthesis and Characterization

2.2.1 Synthesis of ATRP initiators

The ATRP initiators for synthesis of hyperbranched and star-shaped polymers were prepared as described elsewhere [21,23]. For synthesis of 2-(2-bromoisobutyryloxy) ethyl acrylate (BIEA) - an initiator for the hyperbranched polymer preparation, briefly, to a flask containing HEA (9.7 mmol), TEA (10.7 mmol) and THF (15 ml), a solution of BIBB (10.2 mmol) in THF (25 ml) was added dropwise to keep the temperature below 5°C with the help of an ice-water bath. The reaction was run at room temperature for additional 4 h before the formed precipitates were filtered. The filtrate was then concentrated under a reduced pressure to afford a yellowish oil. For synthesis of pentaerythritol tetrakis (2-bromoisobutyrate) or 4-arm BIBB - an initiator for the 4 arm star-shaped polymer preparation, briefly, to a flask containing TEA (10 ml), pentaerythritol (11.0 mmol) and THF (20 ml), a solution of BIBB (81.0 mmol) in THF (25 ml) was added dropwise with stirring at room temperature. After addition was completed, additional 1 h was added to complete the reaction. The solution was washed with 5% NaOH and 1% HCl, followed by extracting with ethyl acetate. The extract was dried with anhydrous $MgSO_4$, concentrated in vacuo and crystallized. The final product was re-crystallized from diethyl ether. The 3-arm and 6-arm initiators were synthesized likewise as described above except that 1,1,1-tris-(hydroxymethyl)-propane and dipentaerythritol were used as a core instead. The synthesis scheme is shown in Fig. 1.

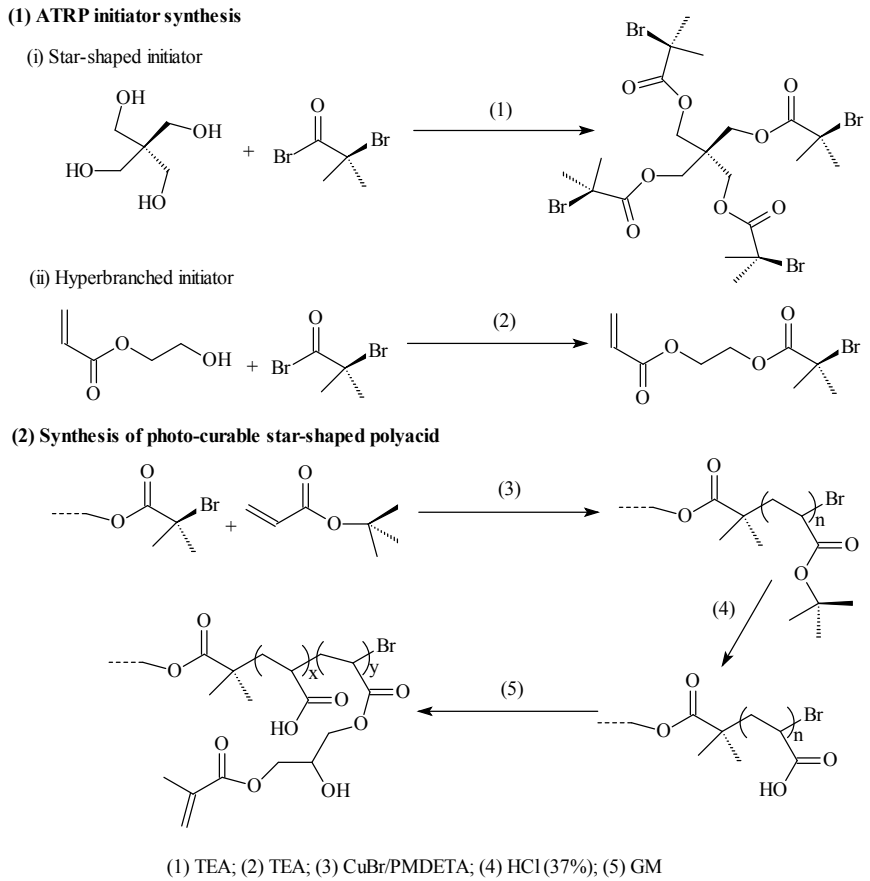

Fig. 1. Reaction scheme: (1) ATRP initiator synthesis: (i) 4-Arm star-shaped initiator BIBB; (ii) Hyperbranched initiator BIEA. (2) Synthesis of photo-curable GM-tethered PAA

2.2.2 Synthesis of the GM-tethered PAA

The GM-tethered poly (acrylic acid) or PAA was synthesized via three steps: synthesis of poly (t-BA) with different molecular architectures via ATRP, conversion of poly (t-BA) to PAA, and tethering of GM onto PAA. (1) For synthesis of poly (t-BA) with different molecular architectures, briefly, to a flask containing dioxane, a mixture of the synthesized ATRP initiator, PMDETA (ligand) and t-BA was charged with a predetermined ratio, where the synthesized ATRP initiator was either 3-, 4-, 6-arm BIBB or BIEA individually for star or hyperbranched PAA, or a combination of 3-, 4- or 6-arm BIBB with BIEA for star-hyperbranched PAA. After the above solution was degassed and nitrogen-purged via three freeze-thaw cycles, CuBr (catalyst) was incorporated. The solution was then heated to 120°C to initiate the ATRP [20,21]. The proton nuclear magnetic resonance (^{1}HNMR) spectrometer was used to monitor the reaction. After the polymerization was complete, the poly (t-BA) polymer was precipitated from water. CuBr and PMDEMA were removed by re-precipitating poly (t-BA) from dioxane/water. (2) For conversion of poly (t-BA) to PAA, poly (t-BA) was hydrolyzed in a mixed solvent of dioxane and HCl (37%, dioxane/HCl = 1/3) under reflux condition for 18 h [20]. The formed PAA was dialyzed against water until the pH

became neutral. The purified PAA was obtained through freeze-drying. (3) For GM tethering [20,21], to a flask containing the synthesized PAA, THF and BHT (inhibitor), a mixture of GM, THF, and pyridine (catalyst) was added dropwise. Under a nitrogen blanket, the reaction was run at 60°C for 5 h and then kept at room temperature overnight. The polymer tethered with GM was recovered by precipitation from diethyl ether, followed by drying in a vacuum oven at room temperature. The overall synthesis scheme is also shown in Figs. 1 and 2 shows the schematic structures of the 4-arm star-shaped, hyperbranched and star-hyperbranched PAA.

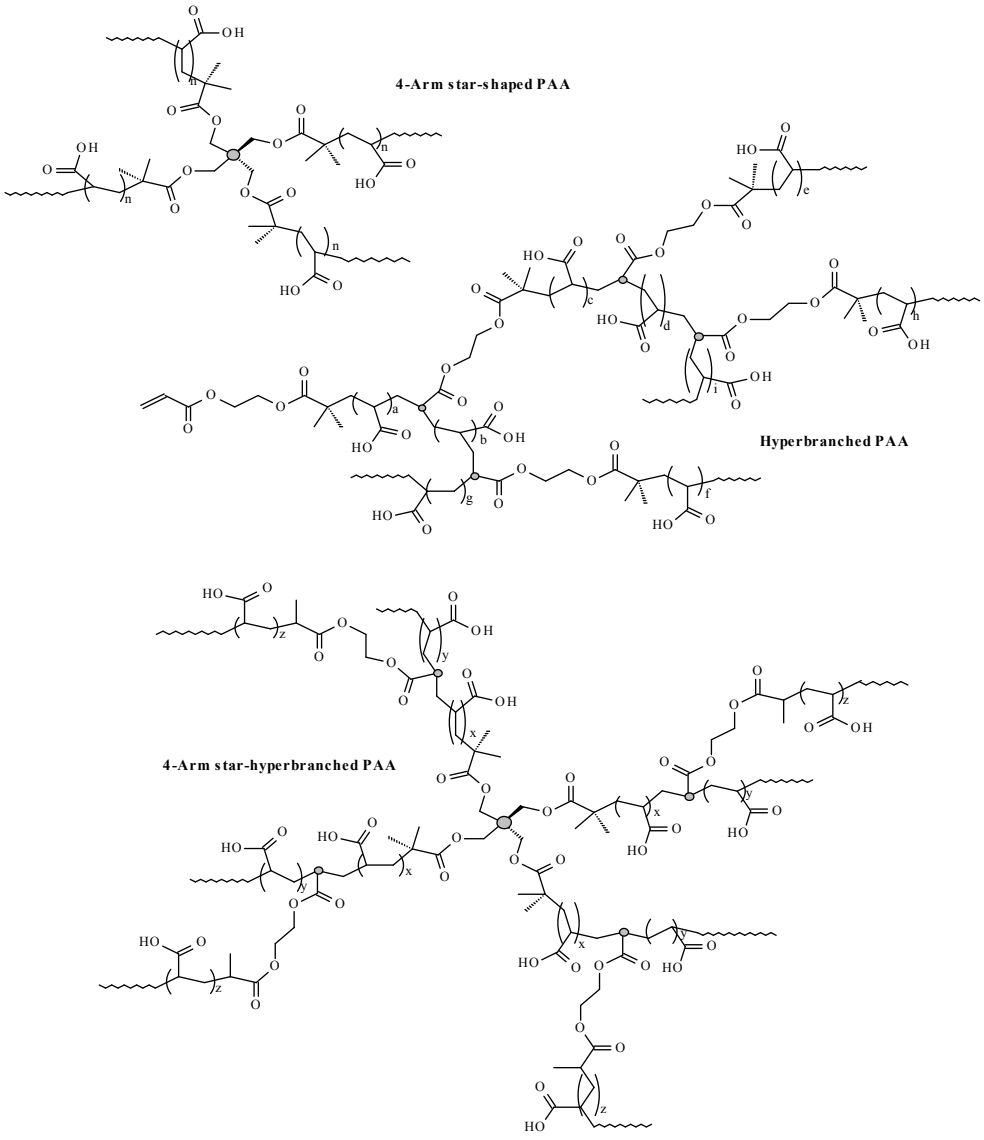

Fig. 2. Structure scheme of star-shaped, hyperbranched and star-hyperbranched PAA

2.2.3 Characterization

The synthesized initiators and polymers were characterized by ^{1}HNMR spectroscopy using a 500 MHz Bruker NMR spectrometer (Bruker Avance II, Bruker Bio Spin Corporation, Billerica, MA). The deuterated methyl sulfoxide (d-DMSO) and chloroform ($CDCl_3$) were used as solvents. The molecular weight (MW) and molecular weight distribution (MWD) of the synthesized poly (t-BA) polymers were determined in THF via a Waters GPC unit (Waters Corp., Milford, MA) with standard GPC techniques, using a polystyrene standard.

The viscosity of the liquid formulated with the polymer and distilled water was determined at 23°C using a cone/plate viscometer (RVDV-II + CP, Brookfield Eng. Lab. Inc., Middleboro, MA).

2.3 Evaluation

2.3.1 Sample preparation

A two-component system (liquid and powder) was used to formulate the experimental cement [22]. The liquid was prepared by dissolving the GM-tethered polymer, CQ (photo-initiator) and DMAEMA (activator) in distilled water where CQ = 0.9% (by weight), DMAEMA = 1.8% and polymer/water (P/W) ratio = 70/30 (by weight). The powder was Fuji II LC glass where glass powder/polymer liquid (P/L) ratio = 2.7. Fuji II LC cement was used as control and prepared per manufacturer's instruction where P/L ratio = 3.2.

Specimens were fabricated at room temperature according to the published protocol [21,22]. Briefly, the specimens were prepared for different tests following the geometries below: (1) cylindrical specimens (4 mm in diameter × 8 mm in length) for compressive strength (CS); (2) disk specimens (4 mm in diameter × 2 mm in thickness) for diametral tensile strength (DTS); (3) rectangular specimens (2 mm in width × 2 mm in thickness × 25 mm in length) for flexural strength (FS); (4) rectangular specimens (4 mm in width × 2 mm in thickness × 20 mm in length), fitted with a sharp blade for generating 2-mm-long notch, for fracture toughness (FT) [24]; (5) disk specimens (4 mm in diameter × 2 mm in height), where the smooth surface at the diametral side was generated by pressing the cement against a microscopic slide before setting, for Knoop hardness (KHN); (6) rectangular specimens (4 mm in width × 2 mm in thickness × 10 mm in length) for wear-resistance; and (7) disk specimens (4 mm in diameter × 2 mm in thickness) for in vitro biocompatibility tests. All the specimens were exposed to blue light (EXAKT 520 Blue Light Polymerization Unit, GmbH, Germany) for 2 min, followed by conditioning at 37°C in 100% humidity for 15 min. Then the specimens for all the mechanical strength tests were conditioned in distilled water for 24 h prior to testing, unless specified. The specimens for in vitro compatibility study were sterilized and prepared for extraction of the leaching components (see in vitro compatibility evaluation under 2.7 for details).

2.3.2 Mechanical property evaluation

CS, DTS, FS, FT, KHN and wear resistance will be used to evaluate the experimental cements. CS is important and very common in dental materials research because many of the forces of mastication are compressive, although it was suggested to be replaced by other tests [25]. DTS is often used for brittle materials because most brittle materials like dental composite and cement are weak in tension. FS is a collective measurement of three types of stress (tension, compression and shear) simultaneously and measurement of FS

offers the best practical and reliable estimate of tensile strength for brittle materials [8]. Hardness is a measure of the resistance to plastic deformation, which is a very common technique to evaluate polymer-containing dental restoratives. Hardness (H) is also sometimes used as an indicator for wear-resistance [26]. Surface hardness correlates well to compressive strength and abrasion resistance [27]. Fracture toughness is a measure of the resistance of a material to crack propagation, which is extremely important to brittle heterogeneous materials because almost every composite material has microcrack tips in the system. A brittle material with higher fracture toughness is expected to have a longer service life. Wear-resistance is a measure of the ability of the material to resist mechanical wear.

CS, DTS, FS and FT tests were performed on a screw-driven mechanical tester (QTest QT/10, MTS Systems Corp., Eden Prairie, MN) with a crosshead speed of 1 mm/min, where the FS and FT tests were conducted in three-point bending, with a span of 20 mm and 16 mm, respectively, between supports. The sample sizes were n = 8 for each material or cement formulation in each test. CS was calculated using an equation of $CS = P/\pi r^2$, where P = the load at fracture and r = the radius of the cylinder. DTS was determined from the relationship $DTS = 2P/\pi dt$, where P = the load at fracture, d = the diameter of the cylinder and t = the thickness of the cylinder. FS was obtained using the expression $FS = 3Pl/2bd^2$, where P = the load at fracture, l = the distance between the two supports, b = the breadth of the specimen, and d = the depth of the specimen. FT was calculated from the equation $K_{IC} = \frac{P \cdot S}{B \cdot W} f(a/W)$, where K_{IC} = the index for FT, P = the load at fracture, S = the distance between supports, a = the length of notch, B = the thickness, and W = the width of specimen. The f is a function of (a/W), as shown below [24].

$$f(x) = \frac{3x^{0.5}[1.99 - x(1-x)(2.15 - 3.93x + 2.7x^2)]}{2(1+2x)(1-x)^{1.5}}$$

The hardness test was performed on a micro-hardness tester (LM-100, LECO Corporation, MI) using a diamond indenter with 25 g load and 30 s dwell time [28]. Knoop hardness number (KHN) was averaged from six readings for each sample.

The wear test was conducted using the Oregon Health Science University (OHSU) oral wear simulator (Proto-tech, Portland, OR) employing ceramic antagonists to produce both abrasive and attritional wear [29,30]. The test was performed following the published procedures [31] with a slight modification. Briefly, after polishing with sand paper, the specimen embedded in the mold was tightened into an individual wear chamber, followed by the addition of a food like slurry consisting of 1.0 g ground poppy seed, 0.5 g PMMA powder and 5 ml distilled water. The abrasion force was set at 20 N and the attrition force at 90 N. The specimen was subject to 70,000 wear cycles at a frequency of 1 Hz. The worn specimen was analyzed using an optical surface profilometer (Surftronic 3+, Taylor Hobson Ltd, Leicester, England) [31]. Both abrasive and attritional wear depths were obtained per manufacturer's recommendation, averaging from three traces. Four specimens were tested to obtain a mean wear value for each material or cement formulation.

2.3.3 *In vitro* biocompatibility assessment

After removing form the molds, the disk specimens were quickly rinsed with 70% ethanol and sterile phosphate buffer saline (PBS), followed by immersing in a 48-well plate

containing 300 µl serum minus DMEM (Dulbecco's modified Eagle's medium or DMEM, Hyclone Laboratories, Inc. Logan, UT) in a humidified incubator at 37°C with 5%CO_2 and 95% air for 1, 3 and 7 days, for preparation of eluates. The surface area to volume ratio was 1 cm^2/ml, which was set according to the ISO standards (0.5-6.0 cm^2/ml) [32]. Five specimens of each material for every eluate preparation were prepared and used for statistical analysis.

Human pulp cells (HPCs) were isolated from the pulp tissue of healthy young permanent teeth undergoing orthodontic treatment, following the published protocol [33]. Briefly, the extracted teeth were cleaned consecutively with sterile PBS, 70% ethanol and PBS, followed by cutting to obtain the pulp tissues. The tissues were then placed in a culture dish and minced to small pieces. Balb/c 3T3 mouse fibroblast cells were obtained directly from the American Type Culture Collection (Manassas, VA).

The cells were then cultured at 37°C in an air atmosphere containing 5% CO_2 and 95% relative humidity, with DMEM containing low glucose, supplemented with 10% heat-inactivated fetal bovine serum (Hyclone Laboratories), 4 mM L-glutamine (Hyclone Laboratories), 100 U/ml penicillin (Sigma-Aldrich, St. Louis, MO), 50 µg/ml gentamicin (Invitrogen Life Technologies, Carlsbad, CA) and 2.5 µg/ml amphotericin B fungizone (Lonza, Walkersville, MD). HPCs which grew out of the explants were sub-cultured and maintained. The HPCs for this study were taken between passage 3 and 8.

In vitro biocompatibility of the experimental cements was evaluated using the water soluble tetrazolium salt (WST) test. The WST was performed as described elsewhere [34,35]. Briefly, the cells were plated in a 96-well plate at 2 x 10^3 cells per well in 100 µl of DMEM supplemented with 10% FBS, 100 U/ml penicillin and 100 µg/ml streptomycin. After incubation at 37°C overnight, the medium was replaced with 100 µl of the fresh medium containing different concentrations of eluate (0, 10, 20, 40, 60 and 80 %). The cells were then incubated for 72 h before the WST testing. The positive control was serum minus DMEM with untreated cells and the negative control was serum minus DMEM without cells. The WST test was conducted by adding 10 µl of WST reagent (Roche Diagnostics, Indianapolis, IN) and 90 µl of serum minus DMEM into a well and then incubating the plate at 37°C for 2 h. The absorbance of the solution was measured at 450 nm using a microplate reader (Molecular devices, Sunnyvale, CA). Cell viability (%) was obtained by the equation: cell viability (%) = (absorbance of the sample elaute - absorbance of the negative control)/(absorbance of the positive control - absorbance of the negative control) × 100%. Cell morphology was obtained at 100X magnification using Nikon eclipse TS100 microscope (Nikon Corp., Japan).

2.3.4 Statistical analysis

One-way analysis of variance (ANOVA) with the post hoc Tukey-Kramer multiple-range test was used to determine significant differences of the measured properties among the materials in each group. A level of $\alpha = 0.05$ was used for statistical significance.

3. RESULTS

3.1 Synthesis and Characterization

3.1.1 Characterization

Fig. 3 shows the ^{1}HNMR spectra of t-BA, 4-arm BIBB, BIEA, star-hyperbranched poly (t-BA), PAA and GM-tethered PAA. The chemical shifts (ppm) were found and listed below: (a) t-BA: 1.50 (-CH_3, 9 H), 5.68 (=CH_2, 1 H), 6.00 (=CHCO-, 1 H) and 6.27 (=CH_2, 1 H); (b) 4-arm BIBB: 1.93 (-$C(CH_3)_2$, 24 H) and 4.32 (CCH_2O, 8 H); (c) BIEA: 1.86 (-CH_3, 6 H), 4.36 (-OCH_2CH_2O-, 4 H), 5.82 (=CH_2, 1 H), 6.08 (=CHCO-, 1 H) and 6.36 (=CH_2, 1 H); (d) poly (t-BA): 1.38 (-CH_3), 1.78 (-CH_2-) and 2.15 (-CHCO-); (e) PAA: 1.51 (-CH_3), 2.36 (-CH_2-), 3.37 (-CHCO-) and 12.24 (-COOH); and (f) GM-tethered PAA: 1.50 (-CH_3), 2.25 (-CH_2-), 3.25 (OH), 3.35 (-CHCO-), 3.80-4.15 (-OCH_2-) 5.67 (CH_2=), 6.06 (CH_2=) and 12.22 (-COOH). The characteristic chemical shifts at 3.25 (OH), 5.67 (CH_2=) and 6.06 (CH_2=) identified the difference between the star-hyperbranched PAA and GM-tethered PAA.

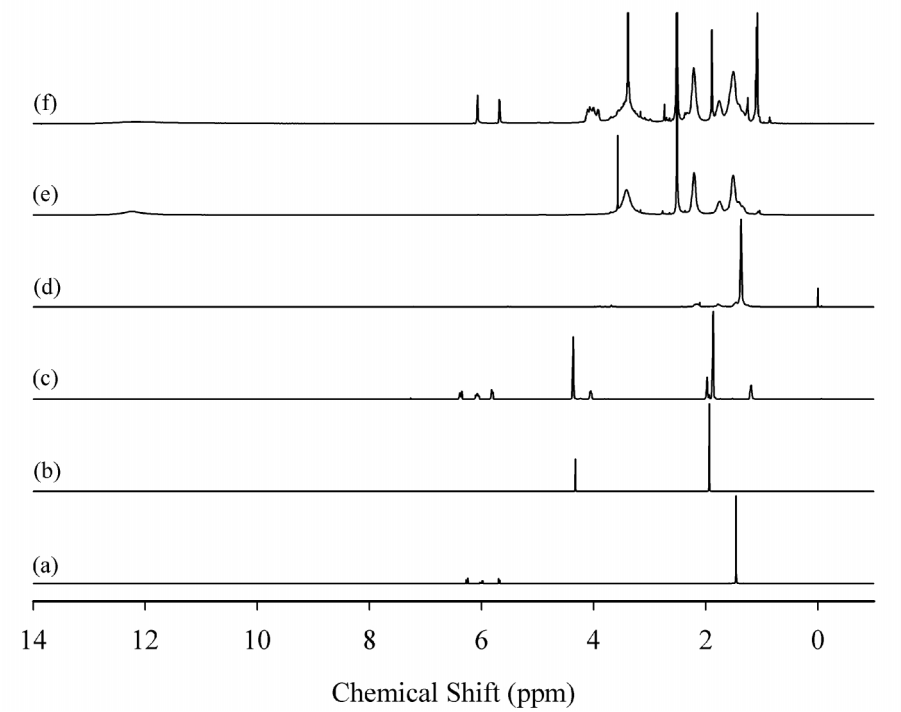

Fig. 3. ^{1}HNMR spectra: (a) t-BA, (b) 4-arm BIBB, (c) BIEA, (d) poly(t-BA), (e) PAA and (f) GM-tethered PAA

3.1.2 Polymerization kinetics

The ATRP polymerization kinetics of poly (t-BA) was studied using ^{1}HNMR. After the polymerization was initiated, aliquots were retrieved from each reaction system at different time intervals, dissolved in $CDCl_3$ and immediately measured with ^{1}HNMR. Fig. 4 shows a set of kinetic plot of monomer to polymer conversion versus time and a semi-logarithmic plot

of ln ($[M]_0/[M]$) versus time, where $[M]_0$ = the initial concentration of the monomer and [M] = the monomer concentration at any time. The conversion was calculated by comparison of the peak integrations between 6.27 (HC=C) and 1.2-1.6 ppm ($-CH_3$). The values of ln ($[M]_0/[M]$) were obtained from ln [1/(1-conversion%)]. Fig. 4a shows a kinetic plot for the 4-arm star-shaped poly (t-BA). Two stages were found from the plot of ln ($[M]_0/[M]$) versus time: a linear plot with 0.682 (slope) and 0.989 (R^2) within 3 h after the reaction was initiated and a deviated plot with a little steeper slope after 3 h. The conversion reached 91, 95 and 97% at 3, 4 and 5 h. Fig. 4b shows a kinetic plot for the hyperbranched poly (t-BA). A similar plot to Fig. 4a is found: a linear plot with 0.486 (slope) and 0.995 (R^2) within 3 h after the reaction was initiated and a deviated plot with a steeper slope after 3 h. The conversion reached 78, 96 and 99.7% at 3, 4 and 5 h, indicating that the reaction was initially slow and then accelerated after 3 h. Fig. 4c shows a kinetic plot for the 4-arm star-hyperbranched poly (t-BA): a linear plot with 0.455 (slope) and 0.957 (R^2) within 3 h and a deviated plot with a steeper slope after 3 h. The conversion reached 78, 98.7 and 99.8% at 3, 4 and 5 h, also indicating that the reaction was accelerated after 3 h.

Fig. 5a shows the effect of the arm number on polymerization kinetics. It was found that each plot remained linear until the ln($[M]_0/[M]$) value exceeded 2.0. The slopes and R^2-values of the linear portions on the curves are 0.838 and 0.999, 2.411 and 0.998, and 4.744 and 0.998 for the ATRP reactions of t-BA initiated with 3-arm, 4-arm and 6-arm initiators, respectively. Fig. 5b shows the effect of the 6-arm initiator concentration on polymerization kinetics. It was found that each plot remained linear until the ln ($[M]_0/[M]$) value exceeded 1.5. The slopes and R^2-values of the linear portions on the curves are 4.744 and 0.998, 1.317 and 0.994, and 0.362 and 0.999 for the 6-arm initiator concentration of 1, 0.5 and 0.25%, respectively.

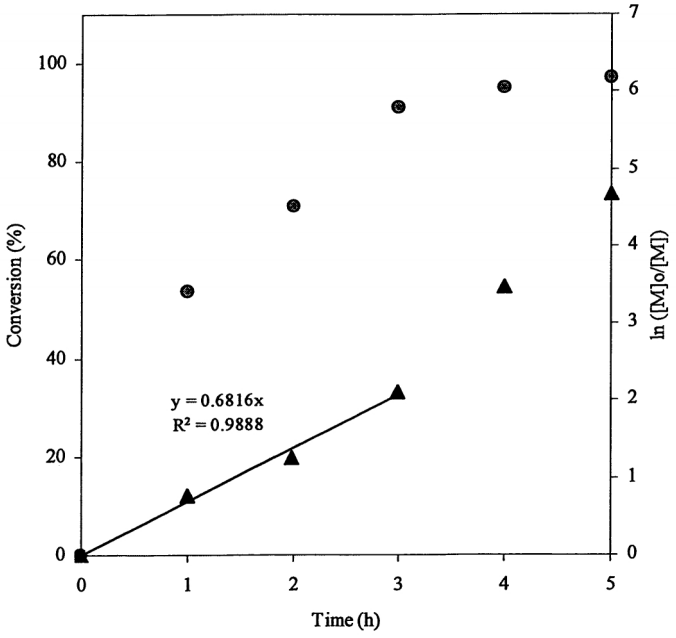

4(A)

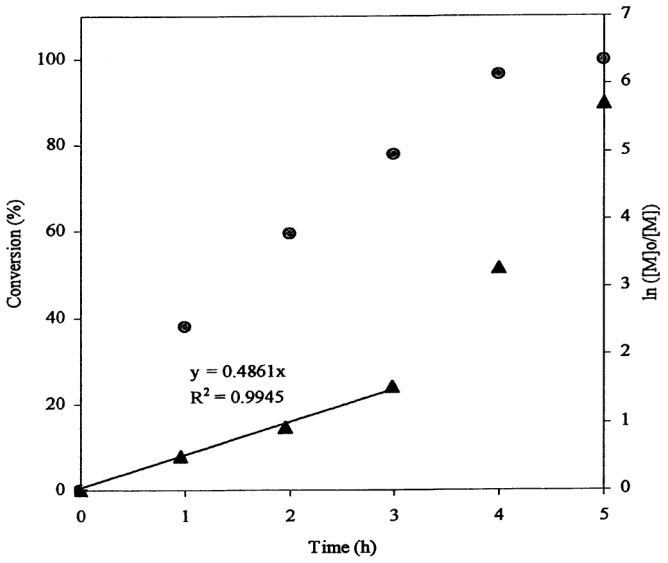

4(B)

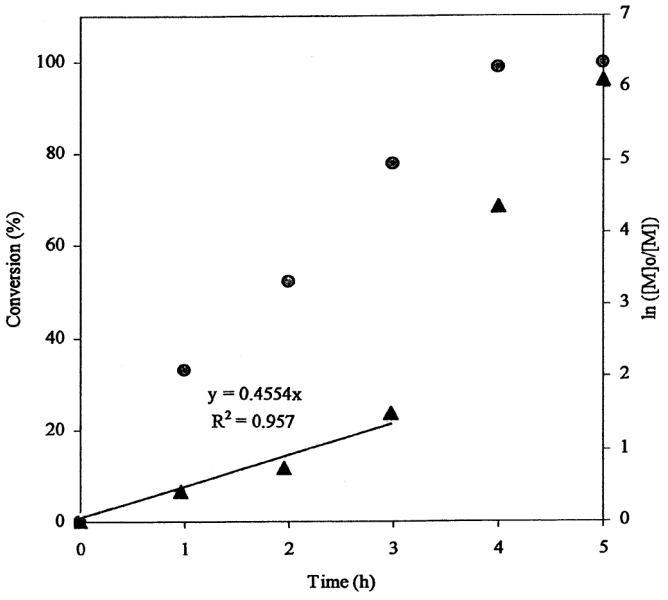

4(C)

Fig. 4. Conversions and kinetic plots of the star-shaped, hyperbranched and star-hyperbranched poly(t-BA) derived from the NMR spectra (upper curve = conversion vs. time and lower curve = ln ($[M]_o/[M]$) verse time): (a) 4-Arm star-shaped poly(t-BA), initiator/t-BA = 0.5% (BIBB); (b) Hyperbranched poly(t-BA), initiator/t-BA = 2% (BIEA); (c) 4-Arm star-hyperbranched poly(t-BA), initiator/t-BA = 0.25% (4-arm BIBB)-1% (BIEA)

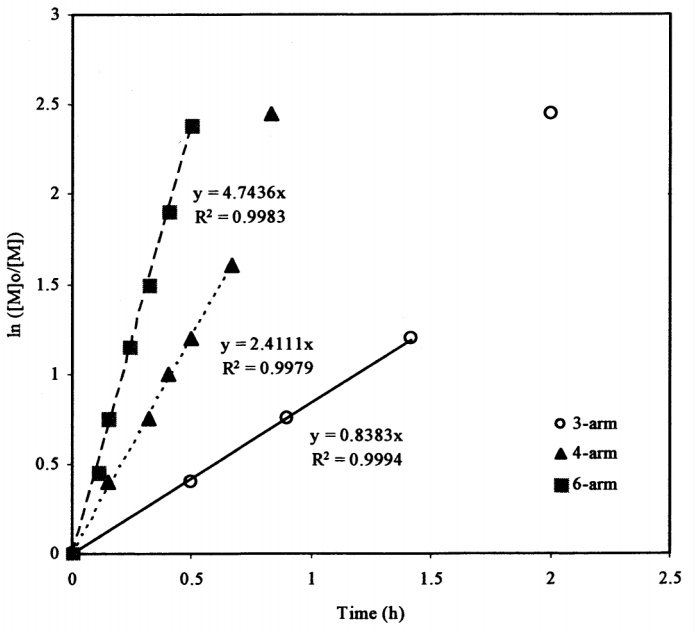

5(A)

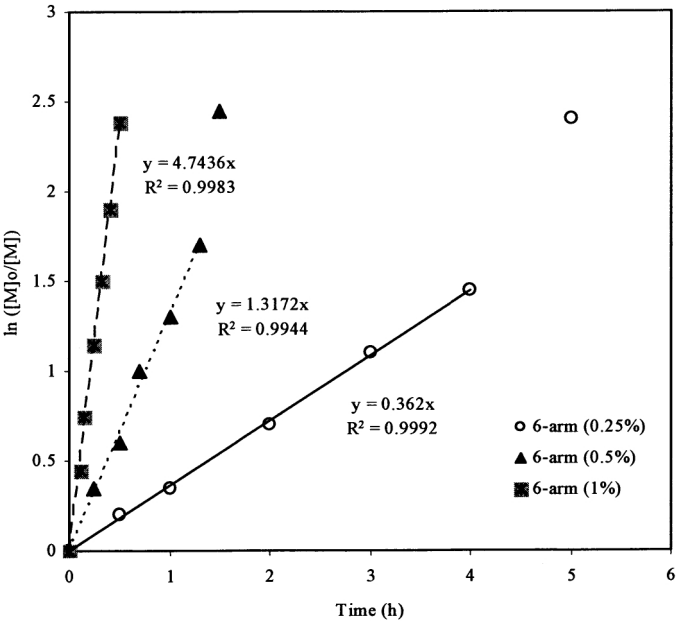

5(B)

Fig. 5. Kinetic plots of ln ($[M]_0/[M]$) verse time for the polymerization of t-BA: (a) Initiation with 3-, 4- and 6-arm initiators: initiator/t-BA = 1% (by mole); (b) Initiation with 0.25%, 0.5% and 1% of 6-arm initiator/t-BA

3.1.3 Effects of the arm number and branching on MW, PDI and viscosity

The measured MW and polydispersity index (PDI) (equivalent to MW distribution) of the synthesized star, hyperbranched and star-hyperbranched poly (t-BA) and the viscosity values of the corresponding PAA aqueous solutions are shown in Table 1. For both star-shaped and hyperbranched polymers, increasing either arm number or branching did not change PDI much but significantly decreased the solution viscosity. For the star-hyperbranched polymers, increasing arm number or branching increased PDI but also decreased the solution viscosity significantly. It is concluded that increasing arm number and branching in the polymer favors a lower solution viscosity.

Table 1. MWs, molecular weight distribution and viscosity of the synthesized polymers[1]

Poly(t-BA)[2]	M_n	M_w	PDI	Viscosity (cp)
Linear control[3]				
Linear (2%)	7550	12653	1.68	N/A
Arm number (S)[4]				
3-star	13081	30086	2.03	1505
4-star	14381	27468	1.91	1157
6-star	15180	28235	1.86	893
Branching (H)[5]				
LDB	46217	138606	3.00	7500
MDB	29718	88057	2.96	5400
HDB	25003	76465	3.06	4102
Arm number (SH)[6]				
3-star	16630	55212	3.32	9270
4-star	17164	49089	2.86	6110
6-star	16725	91988	5.54	4650
Branching (SH)[7]				
LDB	17164	49089	2.86	6110
MDB	12274	46150	3.76	3210
HDB	10575	44204	4.18	1900

[1] M_n, M_w and PDI of poly(t-BA) were measured by GPC, PDI = polydispersity index, and viscosity of the GM-tethered PAA in water (polymer/water or P/W ratio = 60/40, by weight) was determined at 23 °C; [2] S, H and SH = star-shaped, hyperbranched and star-hyperbranched polymers, respectively, LDB, MDB and HDB represent low, medium and high degree of branching; [3] Initiator = 2-bromo-2-methyl-propionic acid methyl ester (2% by mole); [4] Initiator = 3-, 4- or 6-arm star-shaped BIBB (1%); [5] Initiator = BIEA (2%); [6] 3-, 4- or 6-arm star-shaped BIBB (0.125%) + BIEA where BIEA/star-shaped BIBB = 4; [7] Initiators = 4-arm star-shaped BIBB (0.125%) + BIEA where BIEA/star-BIBB = 4, 8 and 16.

3.2 Evaluation

Table 2 shows the effects of the arm number of both star-shaped and star-hyperbranched PAA and branching of both hyperbranched and star-hyperbranched PAA on CS, DTS, FS and compressive modulus of the experimental cements. There seems a trend that increasing the arm number and branching decreased CS, DTS, FS and modulus, although some of the values in each category were not statistically different from one another. Table 3 shows the effects of the arm number and branching of the star-hyperbranched PAA on KHN, FT, abrasion and attrition of the experimental cements. There is also a trend that increasing the arm number and branching decreased KHN, FT, abrasion resistance and attrition resistance,

although some of the values in each category were not statistically different from one another.

Table 2. Effects of arm number and branching on CS, DTS, FS and modulus of the cements

Polymer[1]	CS [MPa]	DTS [MPa]	FS [MPa]	Modulus [GPa][2]
Arm number (S)				
3-star	265.2 (2.1)[3]	43.5 (1.1)[e]	76.3 (3.8)[j]	7.94 (0.11)[n]
4-star	248.4 (13)[a]	39.2 (0.8)[e]	77.4 (1.4)[j]	8.09 (0.20)[n]
6-star	239.1 (11)[a]	32.8 (0.6)	71.5 (0.9)	7.47 (0.14)
Branching (H)				
LDB	325.8 (7.1)	70.4 (5.5)	108.6 (11.2)	7.99 (0.06)
MDB	301.2 (6.9)	51.2 (6.2)	87.8 (4.5)	7.63 (0.13)[o]
HDB	262.2 (12)	26.2 (1.3)	64.2 (2.3)	7.47 (0.32)[o]
Arm number (SH)				
3-star	320.2 (9.4)[b, 3]	72.6 (3.6)[f]	114.2 (14.1)[k]	8.27 (0.10)[p]
4-star	301.7 (9.4)[b, c]	67.9 (2.7)[f, g]	101.4 (7.6)[k, l]	7.95 (0.14)[p, q]
6-star	286.3 (8.9)[c]	58.4 (3.8)[g]	92.4 (11.1)[l]	7.56 (0.22)[q]
Branching (SH)				
LDB	301.7 (9.4)[d]	67.9 (2.7)[h]	101.4 (7.6)[m]	8.27 (0.10)
MDB	285.9 (9.5)[d]	58.8 (3.6)[h, i]	88.4 (9.1)[m]	7.82 (0.14)[r]
HDB	257.8 (10)	49.4 (3.4)[i]	89.1 (15)[m]	7.49 (0.27)[r]

[1]Polymers = GM-tethered 4-arm star-shaped (S), hyperbranched (H), or star-hyperbranched (SH) PAA (see details for the initiators in Table 1), GM grafting ratio = 50% (by mole), P/W ratio = 70/30 (by weight), P/L ratio = 2.7 (by weight); [2]Modulus = compressive modulus; [3]Entries are mean values with standard deviations in parentheses and the mean values with the same letter in each category were not significantly different (p > 0.05). Specimens were conditioned in distilled water at 37 °C for 24 h prior to testing.

Table 3. Effects of arm number and branching on KHN, FT, and wear of the cements

Polymer[1]	KHN	FT [MPa·m$^{0.5}$]	Abrasion [nm·cycle^{-1}]	Attrition [nm·cycle^{-1}]
Arm number (SH)				
3-star	58.9 (3.5)[a, 2]	1.05 (0.06)[c]	0.41 (0.12)	0.71 (0.06)[f]
4-star	58.5 (0.6)[a]	1.11 (0.18)[c]	0.26 (0.05)[e]	0.73 (0.20)[f]
6-star	51.4 (4.3)	1.06 (0.13)[c]	0.26 (0.07)[e]	1.29 (0.32)
Branching (SH)				
LDB	58.5 (0.6)	1.11 (0.18)[d]	0.26 (0.05)	0.73 (0.20)
MDB	49.2 (1.4)[b]	1.11 (0.22)[d]	0.32 (0.06)	0.92 (0.15)
HDB	50.2 (1.4)[b]	1.08 (0.13)[d]	0.56 (0.18)	1.31 (0.30)

[1]Polymers = GM-tethered star-hyperbranched PAA and the details were the same as those shown in Table 2; [2]Entries are mean values with standard deviations in parentheses and the mean values with the same letter in each category were not significantly different (p > 0.05). Specimens were conditioned in distilled water at 37°C for 24 h prior to testing.

Table 4 shows the mean values of CS, modulus, DTS, FS, FT, KHN, abrasion and attrition of the 4-arm star-shaped experimental cement (EXPSGIC), hyperbranched cement (EXPHGIC), and 4-arm star-hyperbranched cement (EXPSHGIC) versus Fuji II LC cement. Apparently, all the experimental cements exhibited significantly higher values than Fuji II LC in all the measured mechanical properties ($p < 0.05$). EXPGICs were 31-53% in CS, 37-55%

in compressive modulus, 80-126% in DTS, 76-94% in FS, 4-21% in FT and 53-96% in KHN higher than Fuji II LC. For wear test, EXPGICs were only 5.4-13% of abrasive and 6.4-12% of attritional wear depths of Fuji II LC in each wear cycle. There is a trend that EXPHGIC showed the highest mechanical strength values, followed by EXPSHGIC, EXPSGIC and Fuji II LC, although there were no statistically significant differences in some of the properties among EXPSGIC, EXPHGIC and EXPSHGIC.

Table 4. Comparison among Fuji II LC and the experimental GICs[1]

Property	Fuji II LC	EXPSGIC	EXPHGIC	EXPSHGIC
CS [MPa]	212.7 (15.0)[2]	277.9 (12)	325.8 (7.1)[a]	320.2 (9.4)[a]
Compressive modulus [GPa]	5.33 (0.09)	7.32 (0.23)	7.99 (0.06)	8.27 (0.1)
DTS [MPa]	31.2 (2.2)	56.2 (0.7)	70.4 (5.5)[b]	67.9 (2.7)[b]
FS [MPa]	55.8 (4.1)	98.4 (5.0)	108.6 (11.2)[c]	101.4 (7.6)[c]
FT [MPa·m$^{0.5}$]	0.94 (0.01)	0.98(0.04)	1.14 (0.02)[d]	1.11 (0.18)[d]
KHN	31.7 (1.0)	48.5 (1.8)	62.1 (3.5)[e]	58.5 (0.6)[e]
Abrasion [nm·cycle^{-1}]	3.90 (0.81)	0.52 (0.07)	0.21 (0.04)[f]	0.26 (0.05)[f]
Attrition [nm·cycle^{-1}]	7.21 (1.99)	0.89 (0.23)	0.46 (0.09)	0.73 (0.20)

[1]Experimental GICs = EXPSGIC (star-shaped), EXPHGIC (hyperbranched) and EXPSHGIC (star-hyperbranched), where all the polymers = GM tethered PAA, GM grafting ratio = 50%, P/W ratio = 70/30 and P/L ratio = 2.7/1, except for the initiators used: 6-arm star-shaped BIBB/t-BA = 1% in EXPSGIC, BIEA/t-BA = 1% in EXPHGIC, and 6-arm star-shaped BIBB (0.25%)-BPEA (1%) in EXPSHGIC; [2]Entries are mean values with standard deviations in parentheses and all the mean values in each category were significantly different ($p < 0.05$). Specimens were conditioned in distilled water at 37°C for 24 h prior to testing.

Fig. 6 shows the cell viability after mouse 3T3 fibroblasts and human pulp cells (HPC) were cultured with the eluates of Fuji II LC and EXPHGIC at a concentration of 80%. For both 3T3 and HPC, EXPHGIC showed the cell viability as close as 100% after cell exposure to 1-, 3- and 7-day eluates. In contrast, Fuji II LC showed the cell viability at 54, 68 and 43% for 3T3, and at 88, 101 and 91% for HPC after cell exposure to 1-, 3- and 7-day eluates.

Fig. 7 shows a set of optical photomicrographs describing both 3T3 and HPC cell morphology after contact with the corresponding 3-day eluates of Fuji II LC and EXPHGIC. In Fig. 7a (HPC only) and 7e (EXPHGIC), numerous healthy cells with an elongated and spindle shape (typical HPC morphology) are observed. However, in Fig. 7c (Fuji II LC), some small black round spots (dead or unhealthy cells) are observed although there still exist many elongated and spindle shaped cells. Likewise, in both Fig. 7b (3T3 only) and 7f (EXPHGIC), numerous cells with a multipolar shape (typical 3T3 cell morphology) are observed and only a few black spots (dead cells) are noticed. In Fig. 7d (Fuji II LC), more black spots and deformed 3T3 cells are observed, although some multipolar-shaped cells are still noticed.

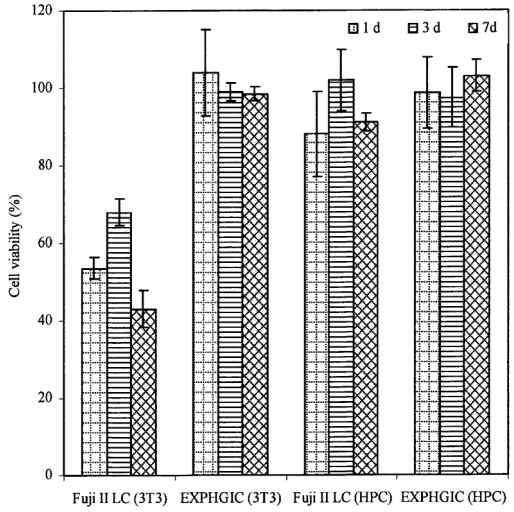

Fig. 6. Cell viability comparison after the cells culturing with the eluates from different cements for 72 h: Fuji II LC (3T3), EXPHGIC (3T3), Fuji II LC (HPC) and EXPHGIC (HPC) stand for Fuji II LC and EXPHGIC eluates culturing with mouse 3T3 fibroblast and human pulp cells, respectively. Eluates were obtained from the 1-, 3- and 7-day incubation at a concentration of 80%

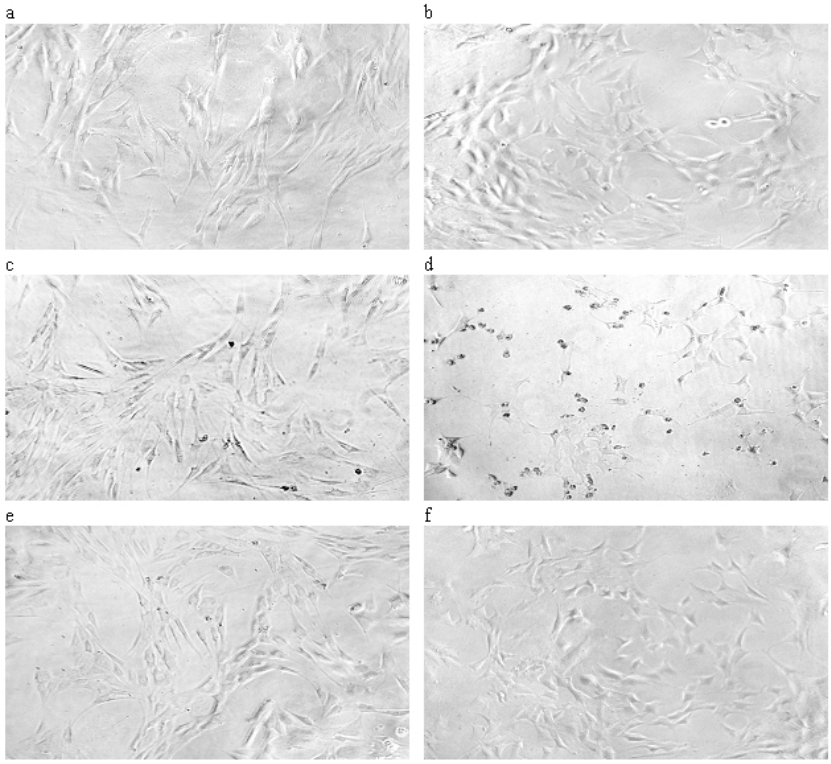

Fig. 7. Cell morphology (100X magnification): (a) HPC; (b) 3T3; (c) Fuji II LC with HPC; (d) Fuji II LC with 3T3; (e) EXPHGIC with HPC; (f) EXPHGIC with 3T3. Cell morphology photomicrograph was obtained after the cells incubating with the 3-day eluates for 72 h.

Fig. 8 shows the effect of aging in water on CS of the experimental cements versus Fuji II LC. Significant increases are observed for all the cements tested from 1 h to 1 d: 17%, 32%, 33% and 32% for Fuji II LC, EXPSGIC, EXPHGIC, and EXPSHGIC. Increases were also found with different aging time: (1) from 1 d to 7 d: Fuji II LC (1%), EXPSGIC (15%), EXPHGIC (4%) and EXPSHGIC (7%); (2) from 1 d to 30 d: Fuji II LC (0%), EXPSGIC (21%), EXPHGIC (8%) and EXPSHGIC (9%).

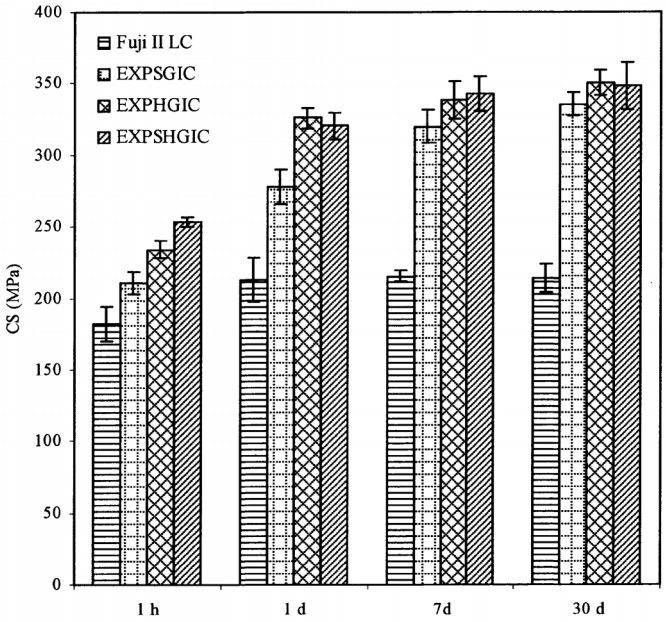

Fig. 8. Effect of aging in water on CS: EXPSGIC, EXPHGIC and EXPSHGIC represent experimental cements composed of the star-shaped, hyperbranched and star-hyperbranched polymers, respectively. The formulations are shown in Tables 2 and 4. All the specimens were conditioned in distilled water at 37 °C prior to testing

4. DISCUSSION

4.1 Polymerization Kinetics

The plot of ln ($[M]_0/[M]$) vs. time can be used to examine whether the reaction follows the first-order kinetics and to calculate the apparent rate constant k or the slop of the plot [36]. It is known that ATRP reaction generally exhibits the first-order kinetics due to persistent radical effect [37] and its kinetic semi-logarithmic plot versus time is expected to be linear. Regarding the polymer synthesis (see Fig. 4), none of these three polymers followed the first-order kinetics. They all went through the two stages, i.e., a linear plot before 3 h and a deviated plot after 3 h. However, compared to the star-shaped PAA (Fig. 4a), either hyperbranched or star-hyperbranched PAA showed a significantly deviated plot from linearity after 3 h with an accelerated polymerization fashion (Figs. 4b and 4c). The plausible reason may be explained below. For synthesis of the star-shaped polymer, a chain grows and extends from each individual reactive BIBB site and thus no branching is expected. However, for synthesis of both hyperbranched and star-hyperbranched polymers, where BIEA was used as an ATRP initiator for branching formation, the case is quite different. At a

lower conversion, a chain growth followed a regular pattern due to a lower viscosity of the reaction system and thus obeys the first order kinetics. At a higher conversion, however, the mobility of the extended polymer chains was significantly reduced due to increased MW and viscosity (In fact, the solution viscosity was observed significantly higher at the later stage). Furthermore, since the acrylate groups on BIEA (ATRP initiator for the hyperbranched polymer synthesis) were located at the end of extended polymer chains, their reactivity as a commoner with the propagating radicals were reduced as well. These two reasons might lead to reduction of the termination constant and thus auto-acceleration of the polymerization. That is why the plot deviated significantly from linearity for synthesis of both hyperbranched and star-hyperbranched polymers. Furthermore, by comparing the slop or k value of the plot, lower values were observed for both hyperbranched (0.486) and star-hyperbranched (0.455) polymer synthesis as compared to the star-shaped (0.682) polymer synthesis, suggesting that at the early stage the propagation of the latter is faster than the former two.

In the case of Fig. 5, all the plots exhibited a high linearity at the early stage of the polymerization (conversion = 80%). The R^2 values (0.994 to 0.999) indicate that the reactivity of the active sites remained constant during this stage. Once the monomer conversion reached 80%, the plot started to deviate from the linearity. This behavior may be explained below: (1) when the conversion was above 80%, the active sites moved to the ends of the long polymer chains, thus limiting their mobility; and (2) the viscosity of the reaction system became higher and higher as the polymer chains grew longer and longer. Both reasons led to reduction of the termination constant, resulting in an accelerated polymerization [38,39].

From Fig. 5a, the slop or k value of the plot for the polymerization was in the decreasing order: 6-arm initiator (4.74) > 4-arm initiator (2.41) > 3-arm initiator (0.838). This can be attributed to the reason that more arms indicate more initiating sites, thus leading to a faster ATRP reaction. From Fig. 5b, apparently the polymerization with a higher initiator concentration showed a higher k value (4.74 for 1%, 1.32 for 0.5% and 0.36 for 0.25%), indicating that the higher the initiator concentration, the faster the ATRP reaction. The results suggest that both arm number and initiator concentration increase the polymerization rate.

4.2 Effects of Arm Number and Branching on MW, MWD and Viscosity

We have studied the effects of arm number and branching on MW, PDI or WMD of the polymers and viscosity of the corresponding PAA aqueous solution (see Table 1). From Table 1, the higher the star arm number, the lower the viscosity is observed, which was demonstrated by either star-shaped PAA or star-hyperbranched PAA. This is logical because the 6-arm star-shaped polymer is even more like a sphere as compared to 3- and 4-arm star-shaped polymers. For the effect of the branching, the higher the degree of branching, the lower the viscosity is observed, which was true for both hyperbranched and star-hyperbranched PAA. It is known in dental clinics that cement mixing requires a workable solution viscosity for the polymer solution. Relatively low solution viscosity favors cement mixing clinically because it can reduce the probability of forming flaws or defects, thus enhancing the mechanical strength [1,2,3,8]. Therefore, without compromising the mechanical strengths a polymer solution with a lower viscosity would be favorable to dental clinics. The results in Table 1 support that branching does decrease the solution viscosity.

4.3 Effects of Arm Number and Branching on Mechanical Properties

The results in Tables 2 and 3 show that there is a trend that increasing either arm number or branching decreased the mechanical strengths, although some changes were not statistically significant. This can be attributed to the fact that all the initiators we used in this study were mainly composed of hydrocarbons and bromoesters (see Figs. 1 and 2). More arms mean more bromoester groups existing in the star-shaped polymers and so do in the hyperbranched polymers. None of these ATRP initiators contain functional groups which could be used for strength enhancement such as carboxyl groups. These bulky hydrophobic initiator cores do not contribute any strength enhancement to the cement system. That may be why the more the initiator in the system, the lower the mechanical strength. Fortunately, these cores did not affect the strength significantly because the initiators used were only 0.25 - 3% by mole.

4.4 Comparison among Experimental Cements and Fuji II LC

We also measured the mechanical properties of commercial Fuji II LC cement and compared them with those for the experimental cements. As shown in Table 4, all the experimental cements showed significantly higher mechanical strengths including CS, compressive modulus, DTS, FS, FT, KHN, abrasion and attrition than Fuji II LC. The higher mechanical strengths exhibited by these EXPGICs can be attributed to the unique nature of the experimental cement system including components, polymer content and the structures of the polymers. As we know, most commercially available systems contain low MW comonomers such as HEMA or methacrylates or dimethacrylates [4,13]. Unlike them, the developed experimental GICs were composed of either star-shaped, or hyperbranched or star-hyperbranched PAA polymer, water and initiators. There were no any low MW comonomers in the experimental cement system. In other words, the experimental cement system essentially is a monomer-free system. The polymer aqueous liquid in the experimental cement system contains highly concentrated GM-tethered PAA, which provides not only a large quantity of carboxyl groups for salt-bridge formation but also a substantial amount of carbon-carbon double bond (methacrylate) for covalent crosslink formation. In contrast, Fuji II LC contains a substantial amount of low MW monomer HEMA (2-hydroxylethyl methacrylate) and other low MW methacrylate or dimethacrylate comonomers, in addition to linear PAA and water [13]. These low MW monomers and oligomers are mainly responsible for the lower strength of the cement.

4.5 *In Vitro* Biocompatibility of EXPGIC versus Fuji II LC

Theoretically speaking, the new experimental cement system is expected to show no cytotoxicity to cells, because it contains no low MW monomers. To confirm this hypothesis, we evaluated the in vitro biocompatibility of EXPHGIC and compared it with Fuji II LC. The results in Figs. 6 and 7 show that the cell viability and morphology of either mouse 3T3 fibroblasts or human dental pulp cells after culturing with the eluates from EXPHGIC were identical to those culturing with only cell culture, suggesting that EXPHGIC is very biocompatible. In contrast, Fuji II LC showed cytotoxicity to both 3T3 and HPC, although it was much worse in the former than in the latter. The reason can be attributed to the fact that Fuji II LC contains 30-35% of HEMA and 5-10% dimethacrylates, which have been proven to be cytotoxic to cells [40,41]. It was also found that 3T3 cells responded more sensitively to Fuji II LC than HPCs.

4.6 Effects of Aging in Water on CS

It is well known that GICs increase their strengths in water with time due to constant salt-bridge formation while water slowly penetrates in [42,43]. To demonstrate the unique nature of the newly developed polymers in the experimental cement system, we measured the CS of the experimental cements versus Fuji II LC after conditioning in water for 1 h, 1 d, 7 d and 30 d (see Fig. 8). Significant CS increases were found for all EXPGICs and Fuji II LC from 1 h to 1 d, indicating that salt-bridge formation mainly occurs during a 24 h period. In addition, huge increase (32-33%) by EXPGICs versus 17% by Fuji II LC indicates that more carboxylic acids exist in EXPGICs than in Fuji II LC. This can be attributed to the fact that EXPGICs contain more PAA than Fuji II LC. The experimental cement system contains 70% GM-tethered PAA and 30% water in liquid whereas Fuji II LC contains 20-30% PAA, 30-35% HEMA, 5-10% dimethacrylates and 20-30% water in liquid [4,13]. After 1 d or 24 h aging, Fuji II LC cement showed almost no change in CS, suggesting that the salt-bridge formation in Fuji II LC was complete within 24 h. This result can be well explained with the composition shown above, i.e., a substantial amount of carboxylic acids for salt-bridges are replaced by HEMA and dimethacrylates in Fuji II LC [13]. On the other hand, a continuous increase in CS by EXPGICs from 1 d to 7 d or even 1 d to 30 d may be partially attributed to the unique star-shaped, hyperbranched or star-hyperbranched molecular structures. We infer that unlike linear PAA, in the star-shaped or hyperbranched or hyperbranched PAA-composed cements, the salt-bridge formation may start gradually from the outside towards inside of the polymer molecules, which requires more time to complete. That is why a continuous increase in CS from 1 d to 7 d or even 30 d was observed.

5. CONCLUSIONS

We have developed and evaluated a novel biocompatible high-strength glass-ionomer cement system composed of PAA with different molecular architectures. These PAA polymers were synthesized via ATRP technique. The results showed that either hyperbranched or star-hyperbranched polymer synthesis proceeds more slowly at the early stage but accelerates more quickly at the later stage than the star-shaped polymer synthesis. The higher the arm number and initiator concentration, the faster the ATRP reaction. It was also found that the higher the arm number and branching that the polymer had, the lower the viscosity of the polymer aqueous solution and the lower the mechanical strengths of the formed cement. The mechanical strengths of all three experimental GICs were very similar to each other but much higher than those of Fuji II LC. The aging study showed that all the experimental cements increased their CS continuously during 30 days, unlike Fuji II LC. This novel cement system was proven to be in vitro biocompatible because it showed no any noticeable cytotoxicity to human dental pulp cells and mouse 3T3 mouse fibroblasts. Future studies will include testing fluoride release, bonding, setting and working time, water-sorption, etc.

CONSENT

Not applicable.

ETHICAL APPROVAL

Not applicable.

ACKNOWLEDGEMENTS

This work was sponsored by NIH challenge grant DE020614.

COMPETING INTERESTS

Authors have declared that no competing interests exist.

REFERENCES

1. Smith DC. Development of glass-ionomer cement systems. Biomaterials. 1998;19(6):467-478.
2. Wilson AD, McLean JW. Glass-ionomer cements. Chicago, IL: Quintessence Publ Co.; 1988.
3. Davidson CL, Mjör IA. Advances in glass-ionomer cements. Chicago, IL: Quintessence Publ Co.; 1999.
4. Wilson AD. Resin-modified glass-ionomer cement. Int J Prosthodont. 1990;3(5):425-429.
5. Hotz P, McLean JW, Sced I, Wilson AD. The bonding of glass-ionomer cements to metal and tooth substrates. Br Dent J. 1977;142(2):41-47.
6. Lacefield WR, Reindl MC, Retief DH. Tensile bond strength of a glass-ionomer cement. J Prosthet Dent. 1985;53(2):194-198.
7. Forsten L. Fluoride release from a glass-ionomer cement. Scand J Dent Res. 1977;85(6):503-4.
8. Craig RG. Restorative Dental Materials. 10th ed. St Louis, MO: Mosby-Year Book, Inc.; 1997.
9. Nicholson JW, Braybrook JH, Wasson EA. The biocompatibility of glass-poly (alkenoate) glass-ionomer cements: a review. J Biomater Sci Polym Edn. 1991;2(4):277-285.
10. Hume WR, Mount GJ. *In vitro* studies on the potential for pulpal cytotoxicity of glass-ionomer cements. J Dent Res. 1988;67(6):915-918.
11. Guggenberger R, May R, Stefan KP. New trends in glass-ionomer chemistry. Biomaterials 1998;19(6):479-483.
12. Mitra SB. Adhesion to dentin and physical properties of a light-cured glass-ionomer liner/base. J Dent Res. 1991;70(1):72-74.
13. Momoi Y, Hirosaki K, Kohno A, Mc Cabe JF. Flexural properties of resin-modified "hybrid" glass-ionomers in comparison with conventional acid-base glass-ionomers. Dent Mater J. 1995;14(2):109-119.
14. Xie D, Culbertson BM, Johnston WM. Formulations of light-curable glass-ionomer cements containing N-vinylpyrrolidone. J M S Pure Appl Chem. 1998;35(10):1631-1650.
15. Xie D, Wu W, Puckett A, Farmer B, Mays J. Novel resin modified glass ionomer cements with improved flexural strength and ease of handling. Eur Polym J. 2004;40(2):343-351.
16. Kao EC, Culbertson BM, Xie D. Preparation of glass-ionomer cement using N-acryloyl-substituted amino acid monomers: evaluation of physical properties. Dent Mater. 1996;12(1):44-51.
17. Xie D, Chung ID, Wu W, Lemons J, Puckett A, Mays J. An amino acid modified and non-HEMA containing glass-ionomer cement. Biomaterials. 2004;25(10):1825-1830.

18. Xie D, Culbertson BM, Johnston WM. Improved flexural strength of N-vinylpyrrolidone modified acrylic acid copolymers for glass-ionomers. J M S Pure Appl Chem. 1998;35(10):1615-1629.
19. Bahadur P, Sastry NV. Principles of Polymer Science. Boca Raton, FL: CRC press, 2002.
20. Huang CF, Lee HF, Kuo SW, Xu H, Chang FC. Star polymers via atom transfer radical polymerization from adamantine-based cores. Polymer. 2004;45(7):2261-2269.
21. Xie D, Park JG, Zhao J. Synthesis and preparation of novel 4-arm star-shape poly (carboxylic acid)s for improved light-cured glass-ionomer cements. Dent Mater. 2007;23(4):395-403.
22. Xie D, Yang Y, Zhao J, Park JG, Zhang JT. A novel comonomer-free light-cured glass-ionomer cement for reduced cytotoxicity and enhanced mechanical strength. Dent Mater. 2007;23(8):994-1003.
23. Zhao J, Xie D. A novel hyperbranched poly (acrylic acid) for improved resin-modified glass-ionomer restoratives. Dent Mater. 2011;27:478-486.
24. Johnson WW, Dhuru VB, Brantley WA. Composite microfiller content and its effect on fracture toughness and diametral tensile strength. Dent Mater. 1993;9(2):95-98.
25. Dowling AH, Fleming GJP, McGinley EL, Addison O. Improving the standard of the standard for glass ionomers: An alternative to the compressive fracture strength test for consideration? J Dent. 2012;40(3):189-201.
26. Forss H, Seppa L, Lappalainen R. *In vitro* abrasion resistance and hardness of glass-ionomer cements. Dent Mater. 1991;7:36-39.
27. Okada K, Tosaki S, Hirota K, Hume WR. Surface hardness change of restorative filling materials stored in saliva. Dent Mater. 2001;17:34-39.
28. Xie D, Brantley WA, Culbertson BM, Wang G. Mechanical properties and microstructures of glass-ionomer cements. Dent Mater. 2000;16(2):129-138.
29. Dowling AH, Fleming GJP. The impact of montmorillonite clay addition on the *In vitro* wear resistance of a glass-ionomer restorative. J Dent. 2007;35(4):309-317.
30. Condon JR, Ferracane JL. Evaluation of composite wear with a new multi-mode oral wear simulator. Dent Mater. 1996;12(4):218-226.
31. Turssi CP, Ferracane JL, Vogel K. Filler features and their effects on wear and degree of conversion of particulate dental resin composites. Biomaterials. 2005;26(24):4932-4937.
32. Lönnroth EC, Dahl JE. Cytotoxicity of liquids and powders of chemically different dental materials evaluated using dimethylthiazol diphenyltetrazolium and neutral red tests. Acta Odontol Scand. 2003;61(1):52-56.
33. Aranha AM, Giro EM, Souza PP, Hebling J, de Souza Costa CA. Effect of curing regime on the cytotoxicity of resin-modified glass-ionomer lining cements applied to an odontoblast-cell line. Dent Mater. 2006;22(9):864-869.
34. Beriat NC, Ertan AA, Canay S, Gurpinar A, Onur MA. Effect of different polymerization methods on the cytotoxicity of dental composites. Eur J Dent. 2010;4(3):287-292.
35. Sun J, Weng Y, Song F, Xie D. In vitro responses of human pulp cells and 3T3 mouse fibroblasts to six contemporary dental restoratives. J Biomater Sci Eng, 2011;4:18-28.
36. Zhao J, Weng Y, Xie D. Synthesis and application of a novel star-hyperbranched poly(acrylic acid) for improved dental restoratives. J Biomater Sci Eng. 2010;3:1050-1060.
37. Matyjaszewski K, Xia J. Atom transfer radical polymerization. Chem Rev. 2001;101(9):2921-2990.
38. Shipp DA, Matyjaszewski K. Kinetic analysis of controlled/“living” radical polymerizations by simulations. 1. The importance of diffusion-controlled reactions. Macromolecules 1999;32:2948.

39. Shipp DA, Matyjaszewski K. Kinetic analysis of controlled/“living” radical polymerizations by simulations. 2. Apparent external orders of reactants in atom transfer radical polymerization. Macromolecules. 2000;33:1553.
40. Geurtsen W, Spahl W, Leyhausen G. Residual monomer/additive release and variability in cytotoxicity of light-curing glass-ionomer cements and compomers. J Dent Res. 1998;77(12):2012-2019.
41. Hanks CT, Strawn SE, Wataha JC, Craig RG. Cytotoxic effects of resin components on cultured mammalian fibroblasts. J Dent Res. 1991;70(11):1450-1455.
42. Cattani-Lorente MA, Godin C, Meyer JM. Mechanical behavior of glass ionomer cements affected by long-term storage in water. Dent Mater. 1994;10(1):37-44.
43. Pearson GJ, Atkinson AS. Long-term flexural strength of glass-ionomer cements. Biomaterials. 1991;12:658-660.

Peer-review history:
The peer review history for this paper can be accessed here:
http://www.sciencedomain.org/review-history.php?iid=446&id=12&aid=3810